JACS
JOURNAL OF THE AMERICAN CHEMICAL SOCIETY

Article

pubs.acs.org/JACS

A Micelle Fusion–Aggregation Assembly Approach to Mesoporous Carbon Materials with Rich Active Sites for Ultrasensitive Ammonia Sensing

Wei Luo,[†,‡] Tao Zhao,[†] Yuhui Li,[‡] Jing Wei,[‡] Pengcheng Xu,[§] Xinxin Li,[§] Youwei Wang,[⊥] Wenqing Zhang,[⊥,▽] Ahmed A. Elzatahry,[#] Abdulaziz Alghamdi,[∥] Yonghui Deng,*[,‡,§] Lianjun Wang,[†] Wan Jiang,[†] Yong Liu,[‡] Biao Kong,[‡] and Dongyuan Zhao*[,‡]

[†]State Key Laboratory for Modification of Chemical Fibers and Polymer Materials, College of Materials Science and Engineering, Donghua University, Shanghai 201620, PR China

[‡]Department of Chemistry, Laboratory of Advanced Materials, State Key Laboratory of Molecular Engineering of Polymers, Shanghai Key Laboratory of Molecular Catalysis and Innovative Materials, Collaborative Innovation Center of Chemistry for Energy Materials (iChEM), Fudan University, Shanghai 200433, PR China

[§]State Key Lab of Transducer Technology, Shanghai Institute of Microsystem and Information Technology, Chinese Academy of Sciences, Shanghai 200050, PR China

[⊥]State Key Laboratory of High Performance Ceramics and Superfine Microstructures, Shanghai Institute of Ceramics, Chinese Academy of Sciences, Shanghai 200050, PR China

[▽]Materials Genome Institute, Shanghai University, Shanghai 200444, PR China

[#]Materials Science and Technology Program, College of Arts and Sciences, Qatar University, PO Box 2713, Doha, Qatar

[∥]Department of Chemistry, College of Science, King Saud University, Riyadh 11451, Saudi Arabia

Supporting Information

ABSTRACT: Nanostructured carbon materials have received considerable attention due to their special physicochemical properties. Herein, ordered mesoporous carbons (OMCs) with two-dimension (2D) hexagonal mesostructure and unique buckled large mesopores have successfully been synthesized via a micelle fusion–aggregation assembly method by using poly(ethylene oxide)-*block*-polystyrene (PEO-*b*-PS) diblock copolymers as a template and resorcinol-based phenolic resin as a carbon precursor. The obtained ordered mesoporous carbons possess unique fiber-like morphology, specific surface area of 571–880 m^2/g, pore volume of 0.54 cm^3/g and large mesopores (up to 36.3 nm) and high density of active sites (i.e., carboxylic groups) of 0.188/nm^2. Gas sensor based on the ordered mesoporous carbons exhibits an excellent performance in sensing NH_3 at a low temperature with fast response (<2 min), ultralow limit of detection (<1 ppm), and good selectivity, due to the large pore sizes, high surface area and rich active sites in the carbon pore walls.

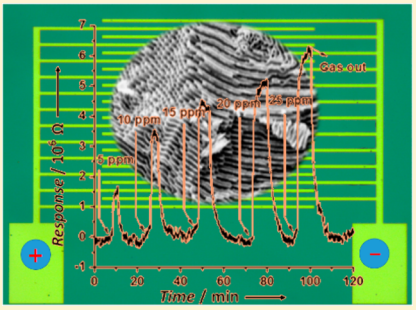

INTRODUCTION

Ammonia is a natural waste product of livestock and the common sources used extensively in manufacturing industries and agriculture. As a highly toxic gas, ammonia can cause irritation to eyes, skin, and respiratory tracts. Additionally, ammonia can react with other air pollutants (NO_x or SO_x) to form particulate matter less than 2.5 μm ($PM_{2.5}$), which can cause lung diseases.[1] A variety of materials has been investigated for the detection of ammonia, such as metal oxides, conducting polymers, and carbon-based materials.[2−10] Gas sensor based on a semiconducting metal oxide relies mainly on continuously monitoring the direct changes of the conductance in adsorption and desorption of NH_3 molecules,[11] including ZnO, SnO_2, WO_3, etc. However, the high operating temperature up to 500 °C and temperature-dependent selectivity limit their applications. Another class of NH_3 sensing materials is conducting polymers like polypyrrole, polyaniline, and polythiophene,[12] and most of them are sensitive to redox-active gases and display changes in electrical resistance as a result of swelling effect in conducting polymer layers.[12] However, the conducting polymers are usually used as dense composite films in gas sensing and exhibit limited sensing performances due to their low surface area.[13] In order to develop high performance ammonia sensors with high sensitivity and short response time at a low temperature, it is highly urgent to explore functional nanostructured materials with a high surface area, good gas diffusion capability, and a numerous exposed active sites.

Received: July 17, 2016
Published: August 30, 2016

DOI: 10.1021/jacs.6b07355
J. Am. Chem. Soc. 2016, 138, 12586−12595

In addition, carbon nanomaterials, such as carbon nanotubes and graphenes, have been demonstrated as promising candidates for ammonia sensing due to good chemical and thermal stability and electronic property, and the sensing mechanism is considered to the charge exchange between carbon nanostructures' surface and the absorbed gas molecules.[7−10,14] As an important kind of nanostructured materials, ordered mesoporous carbon (OMCs) have gained increasing attention in the past ten years due to their outstanding physicochemical properties[15−25] and their wide applications.[26−32] Because of the higher surface area and larger pore volume, OMCs can provide huge interface for the creation of active sites for interaction with ammonia vapor. The periodic porous structure and uniform pore sizes of OMCs can facilitate the diffusion of gas molecules. Lu et al. have fabricated mesoporous-carbon ammonia sensors through a tedious nanocasting approach by using presynthesized mesoporous silica SBA-15 as a hard template and sucrose as a carbon precursor. The obtained OMCs sensors show a good response to ammonia at 50 ppm.[33] However, no work has so far been reported to rationally synthesize OMCs with both large and open mesopores and rich active sites using supermolecular template for high-performace ammonia and other gas sensing.

OMCs are mainly synthesized by using commercial Pluronic type amphiphilic poly(ethylene oxide)-*b*-poly(propyl oxide)-*b*-poly(ethylene oxide) triblock copolymers (e.g., Pluronic P123 and F127) as templates through the synergic coassembly of copolymers an polymerizable precursors (e.g., resol), followed with solidification of the resultant composites and finally selective removal of the templates.[34−39] However, the pore sizes of OMCs are limited to less than 5.0 nm due to the limited molecular weight of Pluronic templates, which greatly hampers their applications. Considerable efforts have recently been made to synthesize ordered mesoporous carbon[40−43] and oxides[44−48] with large mesopores by using homemade block copolymers, such as PEO-*b*-PS, poly(ethylene oxide)-*block*-poly(methyl methacrylate) (PEO-*b*-PMMA), polystyrene-*block*-poly(4-vinylpyridine) (PS-*b*-P4VP). All these syntheses were exclusively accomplished by casting precursor solutions on a substrate to form ordered mesostructures via the conventional solvent evaporation induced self-assembly (EISA) mechanism.[35−37,40−43,47−50] Such a synthesis was accomplished at the solid−liquid interface, which is not scalable and only film or thin plate-like materials can be obtained. However, up to now, it is still a great challenge to realize a solution-phase synthesis of OMCs with pore sizes larger than 5.0 nm and tunable morphologies that are important for their applications.

Previously, amphiphilic PEO-*b*-PS diblock copolymers have been employed as a template to synthesize various ordered mesoporous materials. In most of cases, PEO-*b*-PS block copolymers with a high molecular weight tend to aggregate to form spherical micelles with PS blocks as a core surrounded by PEO shells, especially for the long hydrophobic PS segments, resulting in 3D cubic and cage-like mesoporous structures.[40,41,44,51,52] In very few cases, cylindrical core−shell micelles and 2D hexagonal mesostructure are obtained by controlling the compositional ratio between PEO-*b*-PS block copolymers and precursors, or utilizing mixed precursors.[47,52] The transformation of the mesostructures from 3D cubic to 2D hexagonal may be attributed to the different volume ratio of hydrophilic and hydrophobic parts of PEO-*b*-PS/precursor composites which has effect on the curvature of the block copolymer assemblies.[5]

Herein, we report a facile synthesis of ordered mesoporous carbons with two-dimensional (2D) hexagonal mesostructure, large cylindrical mesopores through a novel solvent evaporation induced micelle fusion−aggregation assembly. It was accomplished through the formation of precipitates by selective evaporation of the tetrahydrofuran (THF) solvent from the basic THF/H_2O solution containing PEO-*b*-PS copolymers as the template, resorcinol-based phenolic resin as carbon precursors, followed by pyrolysis treatment of the precipitate in inert atmosphere. By changing the hydrophobic PS segment length of the template, the mesopore size of the obtained OMCs can be readily tunable from 26.2 to 36.3 nm, and their specific surface area and pore volume can be as high as 571 m^2/g and 0.54 cm^3/g, respectively. More importantly, the OMCs have a high density of active sites (−COOH groups) of about 0.188/nm^2. The obtained OMC materials were employed to fabricate nanodevices as NH_3 sensors which can work at a room temperature and exhibit an excellent sensing performance with a fast response, ultralow limit of detection of 1 ppm, and good selectivity, due to their good merits of large pore size, high surface area, active site-rich pore walls and large pore volumes.

EXPERIMENTAL SECTION

Chemicals and Materials. Monomethoxy poly(ethylene oxide) (Mw: 5000 g/mol) (designed as PEO-5000) was purchased from Aldrich. 2-bromoisobutyryl bromide was purchased from Alfa Aesar. *N*,*N*,*N*′,*N*′,*N*″-Pentamethyl-diethylenetriamine (PMDETA) was purchased from Acros. Copper(I) chloride, Pyridine (AR) and Al_2O_3 (FCP) were purchased from Shanghai Chemical Reagent Co. Ltd. Tetrahydrofuran (THF), ethanol, styrene, anhydrous ethyl ether, petroleum ether (30−60 °C), phenol, resorcinol, formaldehyde aqueous solution (37 wt %) and ammonia−water were AR grade and purchased from Sino-Pharm Chemical Reagent Co. Ltd.

Preparation of PEO-*b*-PS Diblock Copolymers. The amphiphilic PEO-*b*-PS diblock copolymers were prepared by atom transfer radical polymerization (ATRP) method reported previously.[40] The synthesis route involved two steps, (i) the preparation of macroinitiator PEO−Br and (ii) the subsequent polymerization of styrene initiated by PEO−Br. Typically, in the first step, monomethoxy PEO-5000 (20 g) was dissolved in a solvent mixture of THF (60 mL) and pyridine (20 mL). After cooled to 0 °C by ice−water bath, 2-bromoisobutyryl bromide (1.50 g, 6.5 mmol) was added dropwise under stirring for 30 min. The resultant solution was further stirred at 30 °C for 24 h. After a rotary evaporation to remove THF and pyridine, cold ether (200 mL) was added to the solution. The white PEO-Br was precipitated from the reaction solution, washed with cold ether, and dried in vacuum. In the second step, PEO-Br (5.0 g, 1.0 mmol), CuCl (0.10 g, 1.0 mmol), *N*,*N*,*N*′,*N*′,*N*″-pentamethyldiethylenetriamine (0.173 g, 1.0 mmol), and styrene (30.0 g, 288 mmol) were added to an ampules bottle which was then fully degassed with three freeze−pump−thaw cycles and sealed under vacuum. It was subsequently immersed in a thermostated oil bath at 110 °C under stirring to allow polymerization of styrene for 50, 60, 90, and 120 min. The system was then cooled down to room temperature, and the gel like product was dissolved by THF (200 mL). 10 g of Al_2O_3 was added into the resulting solution with stirring for 2 h. The mixture was further filtered through Al_2O_3 column to completely remove the Cu complex. After rotary evaporation to remove THF, petroleum ether (200 mL) was poured into the solution to precipitate PEO-*b*-PS block copolymers. The diblock copolymer product was collected by filtration and dried under vacuum.

Synthesis of Ordered Mesoporous Carbon. The OMCs with 2-D hexagonal mesostructures and large mesopores were synthesized in a basic solution by using THF/H_2O as the mixed solvent, resorcinol and formaldehyde as a carbon source, PEO-*b*-PS diblock copolymers with different molecular weights as a template. For a typical synthesis, PEO_{117}-*b*-PS_{198} (0.045 g) was first dissolved in THF (12 mL) to form

DOI: 10.1021/jacs.6b07355
J. Am. Chem. Soc. 2016, 138, 12586−12595

a clear solution in a glass vial. Then, resorcinol (0.10 g) and water (2.0 mL) was added under magnetic stirring. The obtained transparent solution was allowed to evaporate THF in a hood in air under a mild stirring condition (ca. 100 rpm). After stirring for 3 h, formaldehyde aqueous solution and ammonia−water were added, and the evaporation of THF was kept on under the mild stirring. After evaporation for 30 h, red precipitates of the PEO-*b*-PS/resorcinol−formaldehyde resin composites were collected from the residual suspension (about 3 mL) by centrifugation, followed by washing with water for 5 times, and dried at 60 °C. To remove the copolymer template, the as-made composites were calcined at 600 °C in N_2 for 3 h, giving rise to the mesoporous carbon materials. Through the same approach, PEO_{117}-*b*-PS_{264}, PEO_{117}-*b*-PS_{89} and PEO_{117}-*b*-PS_{97} block copolymers were also used as templates to synthesize mesoporous carbons. The OMC with 3-D cubic mesostructure and large pore size was synthesized similarly to that of the OMCs with 2-D hexagonal mesostructure by using PEO_{117}-*b*-PS_{198} as a template except for the only difference that the evaporation of THF was under static condition.

Gas Sensing Tests. Comb-fingers shaped electrodes were fabricated by using standard microelectro-mechanical system (MEMS) technology and obtained as gifts from State Key Lab of Transducer Technology, Shanghai Institute of Microsystem and Information Technology, Chinese Academy of Science. 0.01 g of the mesoporous carbon samples (carbon-PEO_{117}-*b*-PS_{198}) was added into 1.0 mL of ethanol and homogenized by ultrasonication to form a crude suspension. After that, 0.1 μL of the suspension was loaded onto the comb-like electrode to form a chemiresistor sensor. Then, the electrode sensor was dried in an oven at 80 °C for about 2 h. The sensing response was defined as the resistance change of $\Delta R = R_{NH3} - R_0$. The sensor was operated at room temperature. The NH_3, CH_4, H_2, CO_2, CH_3OH, C_2H_5OH, CH_3COCH_3, benzene and H_2O gas sensing tests were carried out in a lab-made testing chamber (20 L in volume), where the sensor was put inside previously.

Computational Details. The structural and electronic properties were investigated using the plane-wave projector-augmented wave method as implemented in the Vienna ab initio simulation (VASP) package. We employed 2 × 2 × 1 and 8 × 8 × 1 Monkhorst-pack k-meshes for structural relaxation and electronic properties calculations, respectively. Due to the involvement of van der Waals (vdW) interaction, we used the vdW density functional (vdW-DF) in the form of optB86b-vdW for the structure relaxation. The electronic properties were comparatively investigated by using functional Perdew−Burke−Ernzerh (PBE). The supercells contain a vacuum region of at least 12 Å, which was large enough to reduce the periodic interactions between neighboring cells.

Measurement and Characterization. The small-angle X-ray scattering (SAXS) measurements were taken on a Nanostar U SAXS system (Bruker, Germany) using Cu Kα radiation (40 kV, 35 mA). The *d*-spacing values were calculated by the formula: $d = 2\pi/q$. Transmission electron microscopy (TEM) measurements were conducted on a JEM-2100 F microscope (JEOL, Japan) operated at 200 kV. The samples for TEM measurements were suspended in ethanol and supported onto a holey carbon film on a Cu grid. High-resolution scanning electron microscopy (HR-SEM) images were obtained on a Hitachi S4800 field-emission SEM (Japan) operated at 1 kV and 10 μA. The dried samples were directly used for the observation without any treatment. Nitrogen sorption isotherms were measured at 77 K with a Micromeritics Tristar 3020 analyzer (USA). Before measurements, the samples were degassed in a vacuum at 180 °C for at least 6 h. The Brunauer−Emmett−Teller (BET) method was utilized to calculate the specific surface areas using the adsorption data at P/P_0 = 0.02−0.20. The pore size distribution (PSD) was calculated from the adsorption branch by using the Barrett−Joyner−Halenda (BJH) model. The total pore volume (V_{total}) was estimated from the adsorbed amount at P/P_0 = 0.995. The in situ FT-IR measurement was carried out on a Vertex 70v vacuum Fourier transform spectrometer (Bruker, Germany) equipped with a diffuse reflectance accessory (Harrick, USA). Raman spectra were obtained with a Dilor LabRam-1B microscopic Raman spectrometer (France), using a He−Ne laser with an excitation wavelength of 632.8 nm. X-ray photoelectron spectroscopy (XPS) experiments were carried out on a RBD upgraded PHI-5000C ESCA system (PerkinElmer) with Mg Kα radiation ($h\nu$ = 1253.6 eV) or Al Kα radiation ($h\nu$ = 1486.6 eV). Binding energies were calibrated by using the adventitious carbon (C 1s = 284.6 eV). The acidic active sites were analyzed using NH_3-temperature-programmed-desorption (NH_3-TPD) on AutoChem 2920 (USA) apparatus. 50 mg of the sample was loaded in the U-shaped quartz tube and heated at 600 °C for 1 h in helium flow and then cooled to 25 °C for the saturation of the absorbent. NH_3-TPD measurements were carried out in the temperature range of 25−350 °C with a constant heating rate of 10 °C/min.

RESULTS AND DISCUSSION

Amphiphilic high-molecular weight (M_w) PEO-*b*-PS copolymers with the same PEO segment length but different PS chain lengths, i.e., PEO_{117}-*b*-PS_{89}, PEO_{117}-*b*-PS_{97}, PEO_{117}-*b*-PS_{198} and PEO_{117}-*b*-PS_{264}, were prepared via atom transfer radical polymerization (ATRP) approach according to the previous report.[41] In the presence of PEO-*b*-PS templates, the polymerization of resorcinol and formaldehyde catalyzed by ammonia results in reddish PEO-*b*-PS/resorcinol-formaldehyde (RF) precipitate with ordered mesostructure under the continuous evaporation of THF with stirring. After pyrolysis treatment in N_2, the PEO-*b*-PS copolymers can be decomposed and the RF resin can be carbonized, yielding ordered mesoporous carbons (OMCs). By using PEO-*b*-PS copolymers with different molecular weights, a series of OMCs were obtained and denoted as carbon-PEO_x-*b*-PS_y, wherein *x* and *y* represent the numbers of repeating unit of ethylene oxide and styrene, respectively.

The small-angle X-ray scattering (SAXS) patterns of the as-made PEO_{117}-*b*-PS_{198}/RF composites show weak scattering peaks due to the insufficient mass contrast in the organic−organic components (Figure 1a,i). After pyrolysis at 600 °C, the intensity of the scattering peaks (Figure 1a,ii) becomes much strong due to the increase mass contrast, suggesting a formation of the ordered mesoporous structure (carbon-PEO_{117}-*b*-PS_{198}). Three well-resolved scattering peaks at *q* values of 0.256, 0.455, and 0.697 nm^{-1} are observed, which can approximately be indexed as the 100, 110, and 210 reflections of 2D hexagonal mesostructure with the space group *p6mm*. The unit cell parameter (a_0) is calculated to be 28.3 nm (see Table S1), indicative of a large unit of mesostructure. Field-emission scanning electron microscopy (FE-SEM) observation reveals that the as-made PEO_{117}-*b*-PS_{198}/RF resin samples prepared by using PEO_{117}-*b*-PS_{198} as a template have unique fiber-like morphology (Figure 1b), the length of the PEO-*b*-PS/RF fibers is in the range of 5−20 μm. After pyrolysis at 600 °C, ordered mesoporous carbon (carbon-PEO_{117}-*b*-PS_{198}) with typical 2-D hexagonal pattern and long-range regularity can be clearly seen along different directions (Figure 1c−e), due to the removal of the diblock copolymer PEO-*b*-PS templates. Compared to the as-made composites, the ordered mesoporous carbon products show much more clear SEM images due to enhanced conductivity of the samples after the carbonization. The tubular mesopores are estimated to be around 25 nm in diameter according to SEM images, indicating a large mesopores size.

To obtain detailed structure information, the carbon-PEO_{117}-*b*-PS_{198} sample was slightly grinded for transmission electron microscopy (TEM) characterization. The sample shows large-domain regularity, indicating a highly ordered mesostructure (Figure 2a,b). TEM images taken from the [100] and [110] directions with corresponding fast Fourier transform (FFT) diffractograms further confirm a 2-D hexagonal (*p6mm*) symmetry. The cell parameter is estimated from TEM images to be about 28 nm, which is close to the value calculated from

DOI: 10.1021/jacs.6b07355
J. Am. Chem. Soc. 2016, 138, 12586−12595

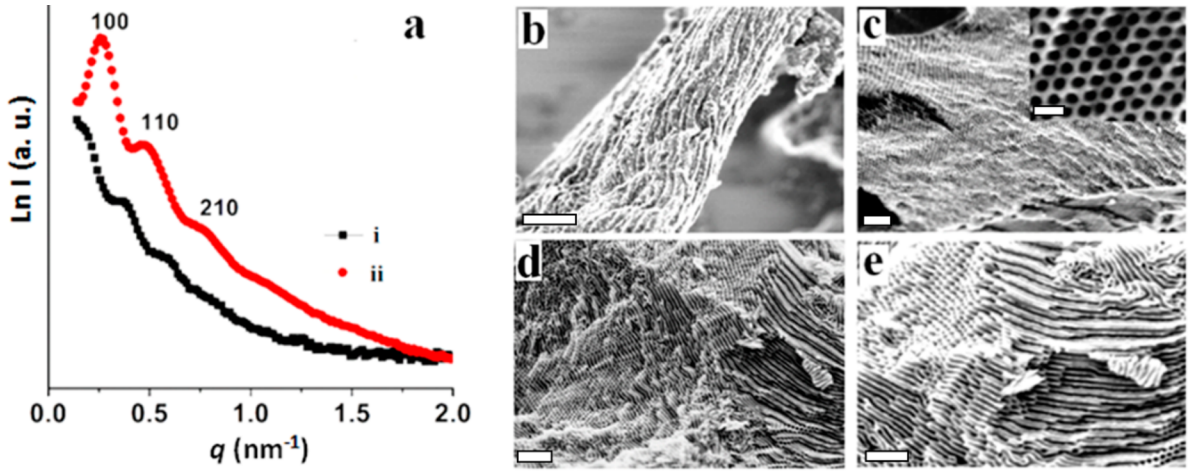

Figure 1. (a) SAXS patterns of (i) the as-made PEO_{117}-*b*-PS_{198}/RF polymer composite prepared by the solvent evaporation induced micelle fusion−aggregation assembly and (ii) ordered mesoporous carbon-PEO_{117}-*b*-PS_{198} obtained after pyrolysis at 600 °C. FESEM images of (b) the as-made PEO_{117}-*b*-PS_{198}/RF composite and (c,d) mesoporous carbon carbon-PEO_{117}-*b*-PS_{198} (e) the magnified image of (d). Scale bars, 1 μm (b), 200 nm (c, d and e), 50 nm (inset in c).

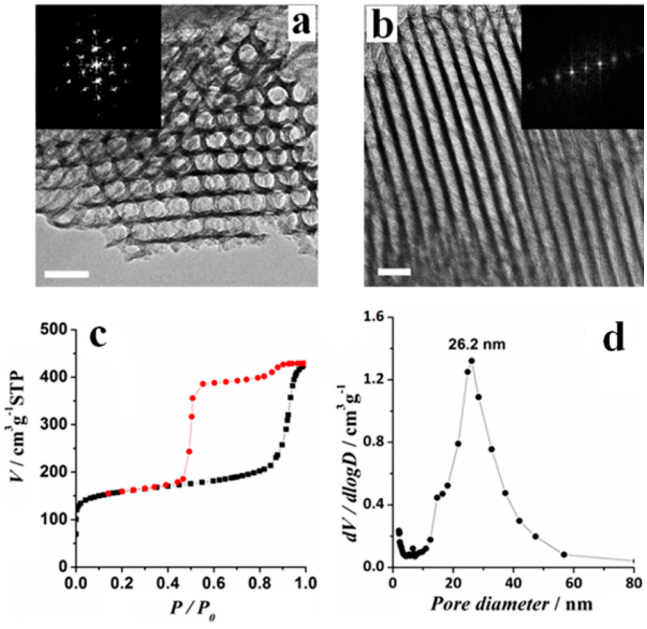

Figure 2. TEM images of the mesoporous carbon-PEO_{117}-*b*-PS_{198} taken along (a) ⟨100⟩ and (b) ⟨110⟩ directions. The insets (a, b) show the corresponding fast Fourier transformation diffractograms. Scale bars, 50 nm. (c) N_2 adsorption−desorption isotherms and (d) the pore size distribution curves of carbon-PEO_{117}-*b*-PS_{198} synthesized by the solvent evaporation induced micelle fusion−aggregation assembly method using PEO_{117}-*b*-PS_{198} as the template after pyrolysis at 600 °C.

the SAXS data. The uniform and large pores with a size of about 26 nm can clearly be observed in the TEM images of the sample carbon-PEO_{117}-*b*-PS_{198} (Figure 2a,b). N_2 sorption isotherms of the mesoporous carbon product, carbon-PEO_{117}-*b*-PS_{198}, templated from PEO_{117}-*b*-PS_{198} copolymers exhibits typical type-IV curves with H1 hysteresis loop. A sharp capillary condensation step is obviously observed in the relative pressure range of 0.87−0.96 (Figure 2c). Such isotherms are not characteristic for typical 2-D hexagonal mesoporous materials (e.g., mesoporous silica SBA-15) but similar to those 2-D hexagonal arrays of buckled cylindrical mesopores with spherical-like mesopores within the channels in domains of the same mass contrast.[53] The desorption branch with slight distortion implies that the pore channels are partially distorted. Therefore, it is speculated that the obtained mesoporous carbon sample (carbon-PEO_{117}-*b*-PS_{198}) consists of cylindrical mesopores with buckled mesochannels. The pore size distribution derived from the adsorption branch using the Barrett−Joyner−Halenda (BJH) method indicates a uniform mesopore of about 26.2 nm (Figure 2d). Taking the cell parameter (a_0 = 28.3 nm) into account, the pore wall thickness of the mesoporous carbon products is calculated to be about 2.1 nm. The BET surface area and total pore volume are calculated to be 555 m^2/g and 0.49 cm^3/g, respectively (Table S1). Raman spectra of the mesoporous carbon (carbon-PEO_{117}-*b*-PS_{198}) show two bands at 1595 and 1314 cm^{-1}, respectively (Figure S1). The first peak can be ascribed to G band related with graphitic sp^2 carbon structures, and the second one stems from D band associated with defective sp^2 carbon structures. Since the G band is relatively weaker than D band, it is concluded that the obtained OMCs are partially graphitized. The XPS measurements of the mesoporous carbon-PEO_{117}-*b*-PS_{198} sample show the chemical state of oxygen on their surface (Figure S2). The high-resolution O 1s spectra can be fitted with three peaks at around 531.6, 533, and 534.6 eV which are attributed to —C═O, C−OH group and chemisorbed oxygen, respectively.[54,55] The C−OH and —C═O groups are mainly from −COOH due to oxidation of resorcinol-based phenolic resins during the pyrolysis treatment. NH_3-TPD profile (Figure S3) of the mesoporous carbon-PEO_{117}-*b*-PS_{198} sample measured in the temperature range of 25−350 °C shows one peak attributed to the desorption of chemically adsorbed ammonia. The amount of NH_3 adsorption is measured to be 3.84 cm^3/g STP, corresponding to a high density of −COOH groups of 0.188/nm^2 by taking the surface area of sample into account.

To investigate the influence of the molecular composition of templates on the mesostructure, PEO_{117}-*b*-PS_{264} and PEO_{117}-*b*-PS_{89} with the same hydrophilic PEO length but different lengths of hydrophobic PS chain were also employed for the synthesis of OMCs under identical conditions through solvent evaporation induced micelle fusion−aggregation assembly method. The SAXS patterns of the obtained mesoporous carbon carbon-PEO_{117}-*b*-PS_{264} are similar to those of carbon-PEO_{117}-*b*-PS_{198},

DOI: 10.1021/jacs.6b07355
J. Am. Chem. Soc. 2016, 138, 12586−12595

and three scattering peaks originated from the 100, 110, and 210 reflections of 2D hexagonal mesostructure (*p6mm*) can clearly be identified (Figure S4a). Due to the longer PS segment length of PEO_{117}-*b*-PS_{264}, the scattering peaks of the sample carbon-PEO_{117}-*b*-PS_{264} shift to lower q values as compared to the sample carbon-PEO_{117}-*b*-PS_{198}. The former has a unit cell parameter of 39.2 nm, much larger than that of the latter (28.2 nm), implying a larger building block formed by PEO_{117}-*b*-PS_{264}. The template with shorter hydrophobic PS segment length results in the mesoporous carbon carbon-PEO_{117}-*b*-PS_{89} with one diffraction peak at a high q value of ~0.34 nm^{-1} (Figure S4b). It indicates a mesostructure with a poor regularity and a small mesostructure feature. FESEM images of the obtained carbon-PEO_{117}-*b*-PS_{264} show ordered mesoporous structure in both the cross section and surface of the sample (Figure 3a,b). The ordered mesostructure can be further verified

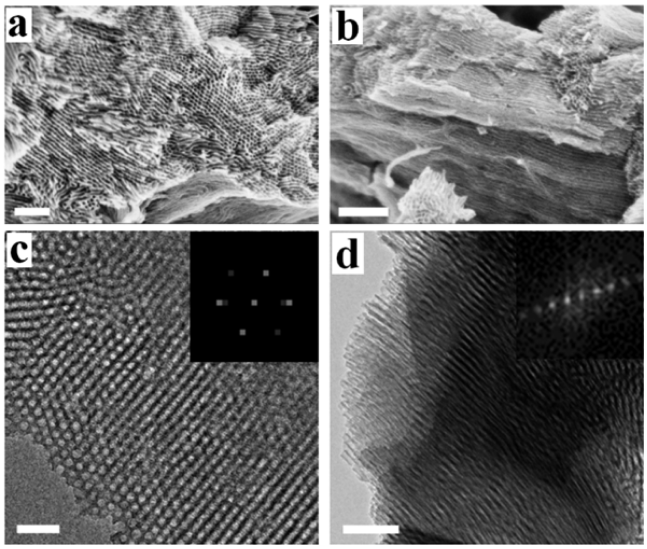

Figure 3. FESEM (a, b) and TEM (c, d) images of the mesoporous carbon carbon-PEO_{117}-*b*-PS_{264} synthesized via solvent evaporation induced micelle fusion−aggregation assembly method after pyrolysis at 600 °C using PEO_{117}-*b*-PS_{264} as the template. The insets (c, d) are the corresponding fast Fourier transformation diffractograms. Scale bars, 200 nm (a, b and d), 100 nm (c).

by the TEM images taken along the ⟨100⟩ and ⟨110⟩ directions, respectively. The diameter of the uniform cylindrical mesopores is roughly measured to be about 35 nm for carbon-PEO_{117}-*b*-PS_{264}, larger than that of carbon-PEO_{117}-*b*-PS_{198} (Figure 3c,d). By contrast, the sample carbon-PEO_{117}-*b*-PS_{89} shows worm-like mesopores with a smaller diameter of about 10 nm, as revealed by the SEM and TEM images (Figure S5a,b). Nitrogen adsorption−desorption measurements show that the samples carbon-PEO_{117}-*b*-PS_{264} and carbon-PEO_{117}-*b*-PS_{89} (Figure S6) have high BET surface areas (571 and 880 m^2/g), large total pore volumes (0.54 and 0.59 cm^3/g), and uniform pore sizes (36.3 and 10.9 nm), respectively. All these results clearly indicate that the templates with longer hydrophobic PS chains result in larger mesopores, and the PEO_{117}-*b*-PS_{89} template with too large hydrophilic/hydrophobic ratio is unfavorable for the construction of ordered mesostructure.

In order to verify the effect of gentle stirring, mesoporous carbon materials were also synthesized via the same approach and condition with that for the sample carbon-PEO_{117}-*b*-PS_{198} but without stirring by using amphiphilic diblock copolymer PEO_{117}-*b*-PS_{198} as a template (denoted as carbon-PEO_{117}-*b*-PS_{198}-static). N_2 sorption isotherms (Figure S7a) of the control sample carbon-PEO_{117}-*b*-PS_{198}-static exhibits representative type-IV curves with a sharp capillary condensation step in the relative pressure range of 0.85−0.95. It indicates the generation of uniform mesopores with an ultralarge size. A very large H1-type hysteresis loop with delayed capillary evaporation located at a relative pressure of about 0.45 is observed, implying that the carbon materials possess a large pore volume. The pore size distribution derived from the adsorption branch using the BJH method (inset in Figure S7a) shows that the pore size is uniform and centered at about 24 nm, close to the pore diameter of the sample carbon-PEO_{117}-*b*-PS_{198}, because of the same template employed in the both samples. The BET surface area and total pore volume is calculated to be 432 m^2/g and 0.59 cm^3/g, respectively. The SAXS pattern (Figure S7b) of carbon-PEO_{117}-*b*-PS_{198}-static shows three scattering peaks with q-values of 0.31, 0.48, and 0.62 nm^{-1}, respectively, which can be indexed as the 111, 311, and 331 reflections of ordered 3-D face centered cubic closed-packing (*fcc*) mesostructure with the space group of $Fm\bar{3}m$. The FESEM image (Figure S7c) clearly indicates that the sample carbon-PEO_{117}-*b*-PS_{198}-static has a high degree of periodicity over large domains. TEM images (Figure S7d−f) further confirm the formation of large-domain ordered cubic mesostructure with large pores viewed from the 100, 110, and 211 directions of $Fm\bar{3}m$ symmetry. These results clearly indicate that the sheering stress plays an important role in the formation of 2D hexagonal mesostructures.

To gain further insight about the coassembly of PEO-*b*-PS and RF resin, intermediate samples were withdrawn during THF evaporation from the basic THF/H_2O solution containing PEO_{117}-*b*-PS_{189}, resorcinol and formaldehyde. After evaporation of THF for 5 h under stirring, numerous randomly dispersed nanowires with a length of 50−200 nm and diameter of about 30 nm, accompanying with nanospheres of about 30 nm, can be clearly seen in the SEM image (Figure 4a). Many nods can be

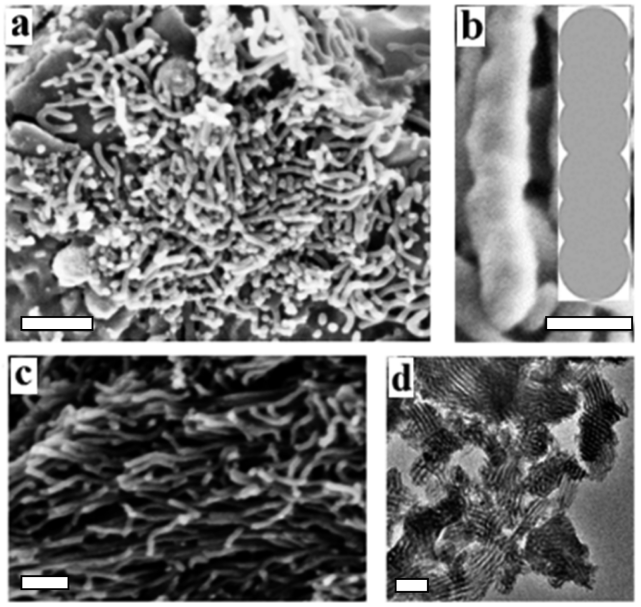

Figure 4. (a, b) SEM images of the intermediate composite PEO_{117}-*b*-PS_{198}/RF sample withdrawn from the synthesis batch after the evaporation of THF for 5 h. (c) SEM and (d) TEM images of the intermediate sample withdrawn after the evaporation of THF for 15 h. Scale bars are 200 nm (a), 50 nm (b) 100 nm (c), 200 nm (d).

DOI: 10.1021/jacs.6b07355
J. Am. Chem. Soc. 2016, 138, 12586−12595

observed along the nanowires in the magnified SEM image (Figure 4b). These results imply that the spherical PEO-*b*-PS/RF composite micelles are formed initially, which may experience the attachment and fusion along one direction to form 1D nanowires because of the shear force from stirring. With a continuous evaporation of THF for 15 h, longer nanowires can be obtained, which tend to coassemble into ordered mesostructure in some domains (Figure 4c). After pyrolysis at 600 °C, the obtained intermediate sample shows 2D ordered arrays of cylindrical mesopores in small domains (Figure 4d), suggesting that the intermediate rod-like composite nanowires could further assemble to ordered mesostructure.

On the basis of the above results, we proposed a solvent evaporation induced micelle fusion−aggregation assembly process for formation of the 2D hexagonal mesoporous carbon materials (Figure 5). In the beginning, the high-molecular weight and water-insoluble PEO-*b*-PS templates can be well dissolved in THF/H_2O solution with a very high volume ratio of THF/water (6:1), because THF is a good solvent for the diblock copolymer templates. With the evaporation of THF, the solubility of the mixed solvent for PEO-*b*-PS copolymers decreases gradually because water is a poor solvent for the PS segments, but good solvent for PEO segments. It induces the micellization of the copolymers into nanospheres with a PS core solvated by THF and a PEO shell contacting both water and THF (Step 1). After introducing resorcinol, resorcinol molecules can interact with the PEO moieties via hydrogen bonding between the ether bond and hydroxyl groups of phenols (Step 2). With the sheering stress of the gentle stirring and introduction of formaldehyde and ammonia−water, the spherical micelles can be slightly fused along one direction and tend to form 1D bamboo-joint-like nanorods and even nanowires when more and more micelles are formed upon the continuous loss of THF. On the other hand, the polymerization of resorcinol and formaldehyde around the composite quasi-cylindrical micelles leads to cylindrical core−shell micelles with bamboo-joint-like PS microdomains covered by the PEO/RF resin composites between the THF-rich and water-rich phases (Step 3). As the composite micelles become concentrated with continuous evaporation of THF, they coassemble into ordered mesostructure driven by the balance of repulsion force of negatively charged rods and the van der Waals attraction force, resulting in reddish precipitate from the residual solution. The ordered mesostructure can be finally solidified by RF polymer as their cross-linking density is further increased upon heating (Step 4). After final pyrolysis at a high temperature in N_2, the template can be decomposed, leaving 1D buckled mesopore channels; while the RF resin can be carbonized into carbon framework with partially graphitized structure (Step 5).

It is worth noting that this solvent evaporation induced micelle fusion−aggregation assembly method can be extended for other materials with similar 2D hexagonal mesoporous structure and large mesopores. For example, by using PEO_{117}-*b*-PS_{198} as a template, mesoporous carbon-silica hybrid composites with a large tubular pore of 27.2 nm can obtained by introducing tetraorthosilica (TEOS) in the synthesis system (Figure S8, S9). When only TEOS was used as the precursor, ordered mesoporous silica with a pore size of 33.0 nm can be obtained (Figure S10, S11). Due to their high surface area and large pores, these materials are useful in various applications involving large size guest molecules and nanoparticles.

The nanostructured carbon materials reported previously, including carbon nanotubes and graphene, have been shown to response to the changes of concentration of volatile chemicals through the susceptibility of their electronic structures upon contacting molecules.[56−58] These materials are usually considered as p-type semiconductors with holes acting as charge carriers. When typical electron donor molecules like NH_3 are adsorbed on carbon materials, the concentration of holes in valence band decreases and thereby results in an increased resistance of carbon materials. Herein, encouraged by the high surface area of our OMCs with ultralarge mesopores and

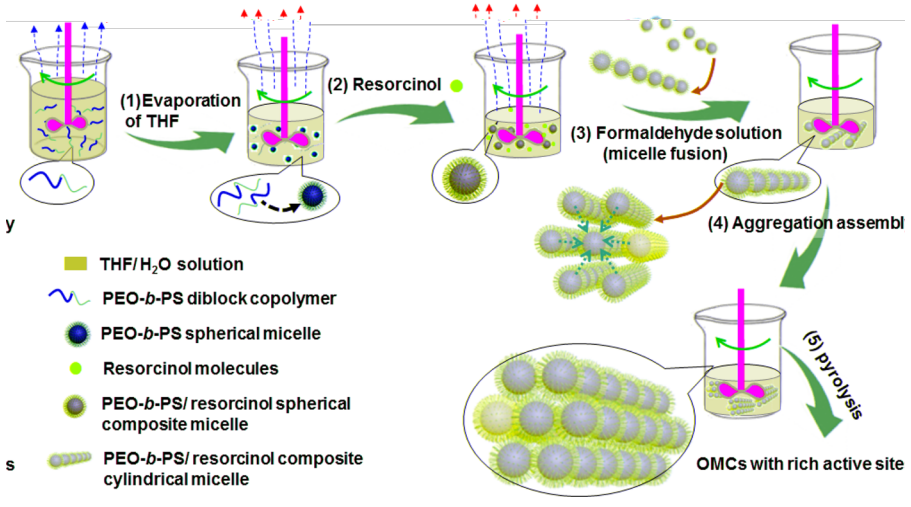

Figure 5. Proposed formation mechanism of the mesoporous carbon materials with ultralarge buckled mesopores via the solvent evaporation induced micelle fusion−aggregation assembly method using PEO-*b*-PS as the template, resorcinol and formaldehyde as the carbon source and THF/water as the solvent. **Step 1**. With the evaporation of THF, PEO-*b*-PS copolymers self-organize into micellar nanospheres with a PS core and a PEO shell in the solution. **Step 2**. After introduction of resorcinol, resorcinol molecules interact with the PEO moieties via hydrogen bonding between the ether bond and hydroxyl groups of phenols. **Step 3**. With the sheering stress of the gentle stirring and the introduction of formaldehyde and basic catalyst, the spherical micelles are slightly fused into bamboo-joint-like 1D nanorods upon the continuous loss of THF, and the polymerization of resorcinol and formaldehyde around the composite micelles fix the cylindrical core−shell micelles with PS microdomains covered by the PEO/RF resin composites. **Step 4**. The composite micelles assemble into an ordered mesostructure and precipitate from the residual reaction solution. **Step 5**. Ordered mesoporous carbon materials with large mesopores are finally obtained after pyrolysis treatment of the collected precipitates.

DOI: 10.1021/jacs.6b07355
J. Am. Chem. Soc. 2016, 138, 12586−12595

plentiful active sites, we investigated the performance of the mesoporous carbon-PEO$_{117}$-*b*-PS$_{198}$ for NH_3 gas sensing at room temperature. The NH_3 sensor device was fabricated by positioning a layer of OMCs paste on the interdigital electrodes (Figure 6a,b). The sensor exhibits a sharp increase of resistance upon contact NH_3 of a low concentration in the range of 5−25 ppm (Figure 6c), lower than the maximum concentration allowed for exposure at the working place (25 ppm).[59] Even when a low dose (5 ppm) of NH_3 is input, the response can reach ∼1.6 MΩ, which is 4.4 times larger than the noise-floor (±0.18 MΩ calculated from the baseline). After vacancy, the resistance can be recovered to its initial value for all the testing concentrations, reflecting a good reversibility of the gas sensor. Surprisingly, the minimum detectable concentration can reach as low as 1 ppm. Besides, the sensor shows a quick response to 5 ppm of NH_3 in 2 min and recovers in 4 min. These results clearly indicate that our ordered mesoporous carbons have an ultrahigh sensitive performance, although it follows the same NH_3-sensing mechanism for other carbon-based nanomaterials such as CNTs and graphene,[10,14] that is, the resistance increases upon contact with NH_3. Compared to the carbon-based sensors reported previously,[7−10,60−69] our OMC sensor can detect much lower NH_3 concentration within shorter response time due to their large mesopores, good diffusion property and abundant active sites. More importantly, OMC sensors show an output of about 5 MΩ to NH_3 of 20 ppm, much larger than the values (below 1 MΩ) for the seven common interfering gases with identical centration of 20 ppm, including methane, hydrogen, carbon dioxide, methanol, ethanol, acetone, and benzene (Figure 6d). It indicates that our large-pore mesoporous carbon sensor has an excellent sensing selectivity. Under normal circumstances, our sensor works under the environmental humidity of 30−70%. In order to verify the effects of the relative humidity changes to sensing performance, the sensing responses of our OMC sensor to water vapor were studied.

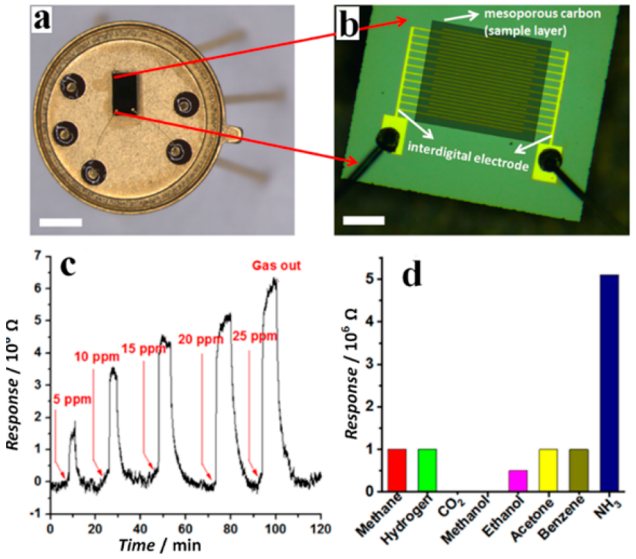

Figure 6. (a) Optical microscopy image of the sensing device with its interdigital electrode (b) covered by the large-pore mesoporous carbon films. (c) The response and recovery curve of the large-pore mesoporous carbon carbon-PEO$_{117}$-*b*-PS$_{198}$ sensor to NH_3 at different concentrations (5−25 ppm) at room temperature. (d) Responses of the mesoporous carbon carbon-PEO$_{117}$-*b*-PS$_{198}$ sensor to different gases with a concentration of 20 ppm. Scale bars, 2 mm (a), 200 μm (b).

As shown in Figure S12, the sample carbon-PEO$_{117}$-*b*-PS$_{198}$ as a sensing material generates negligible response to the water vapor (1725 ppm), due to the hydrophobic characteristic of our OMCs. The results show a great promise of our sensor in resisting the noise from humidity fluctuation.

For comparison with our large-pore OMC (carbon-PEO$_{117}$-*b*-PS$_{198}$), two kinds of OMCs were synthesized and tested for NH_3 sensing. One is the conventional mesoporous carbon C-FDU-15 templated from Pluronic copolymers, and another is carbon-PEO$_{117}$-*b*-PS$_{97}$ templated from diblock copolymer PEO$_{117}$-*b*-PS$_{97}$ with a lower molecule weight. C-FDU-15 and carbon-PEO$_{117}$-*b*-PS$_{97}$ have similar 2-D hexagonal mesopore structure and surface areas (567 and 558 m^2/g, respectively), smaller pore size (3.3 and 13.8 nm, respectively), and slightly lower density of −COOH groups (0.083 and 0.131/nm^2, respectively). It was found that their discriminated detectable concentrations were located around 15 ppm (i.e., the detection limit of C-FDU-15 and carbon-PEO$_{117}$-*b*-PS$_{97}$ was around 15 ppm, Figure S13 and S14), much higher than that (1 ppm) of our carbon-PEO$_{117}$-*b*-PS$_{97}$ samples. In addition, the response and recovery time of the C-FDU-15 based sensor to NH_3 input of 15 ppm exceeded 7 and 15 min, respectively (Figure S13). The carbon-PEO$_{117}$-*b*-PS$_{97}$ based sensor exhibited almost the same recovery time (15 min, Figure S14), but shorter response time (6 min, Figure S14). These results clearly indicate that our mesoporous carbon products carbon-PEO$_{117}$-*b*-PS$_{198}$ with a larger pore size possess much better performance in NH_3 sensing. Comparatively, the carbon-PEO$_{117}$-*b*-PS$_{198}$-static sample was found to have a detection limit of around 30 ppm, indicating a much poor sensing performance due to the small pore opening (i.e., window) and thick pore walls of the *fcc* mesostructure made of spherical pores.

In the sensing performance tests, the interaction between ammonia and mesoporous carbon depends on the active adsorption sites at the surface of the carbon pore walls. As shown in Table S2, we employed pure tetragonal amorphous graphite, defect graphite surface, hydroxyl (−OH), carboxyl (−COOH) and ketone (—C═O) to theoretically investigate the adsorption performance. The absorption energy (E_{abs}) of NH_3 on the surface or with the groups mentioned above can be calculated by the following equation:

$$E_{abs} = -(E_{NH3+C} - E_{NH3} - E_C)$$

where E_{NH3} and E_C is the molecular energy of individual NH_3 and corresponding carbon matrix; E_{NH3+C} is the molecular energy of the carbon matrix absorbed by NH_3. According to the calculations, the mesoporous carbon as NH_3 sensors is independent of the amorphous graphite, defect sites and —C═O groups, which attribute to the rather small absorption energy, only in ∼10^{-2} eV (0.07, 0.04, 0.04 eV, respectively, Table S2), indicating the weak physical adsorption between them and NH_3 molecules. In contrast, absorption energy between −OH, −COOH groups and NH_3 molecule (0.40, 0.51 eV, respectively, Table S2) is large enough to prove the existence of strong chemical adsorption. Based on the theoretical calculations, it can be concluded that the strong absorption between NH_3 and hydroxyl sites (−OH or −COOH) is ascribed to the chemical bonds form of ammonium-salt NH_4^+. As shown in Figure 7, the widths of upper valence band of NH_3 in the two cases (mesoporous carbon with −OH and −COOH at surface, respectively) are about 3 eV under the top of valence band, instead of the localized states in the three cases (mesoporous carbon with graphite-structured surface, defected surface and —C═O

DOI: 10.1021/jacs.6b07355
J. Am. Chem. Soc. 2016, 138, 12586−12595

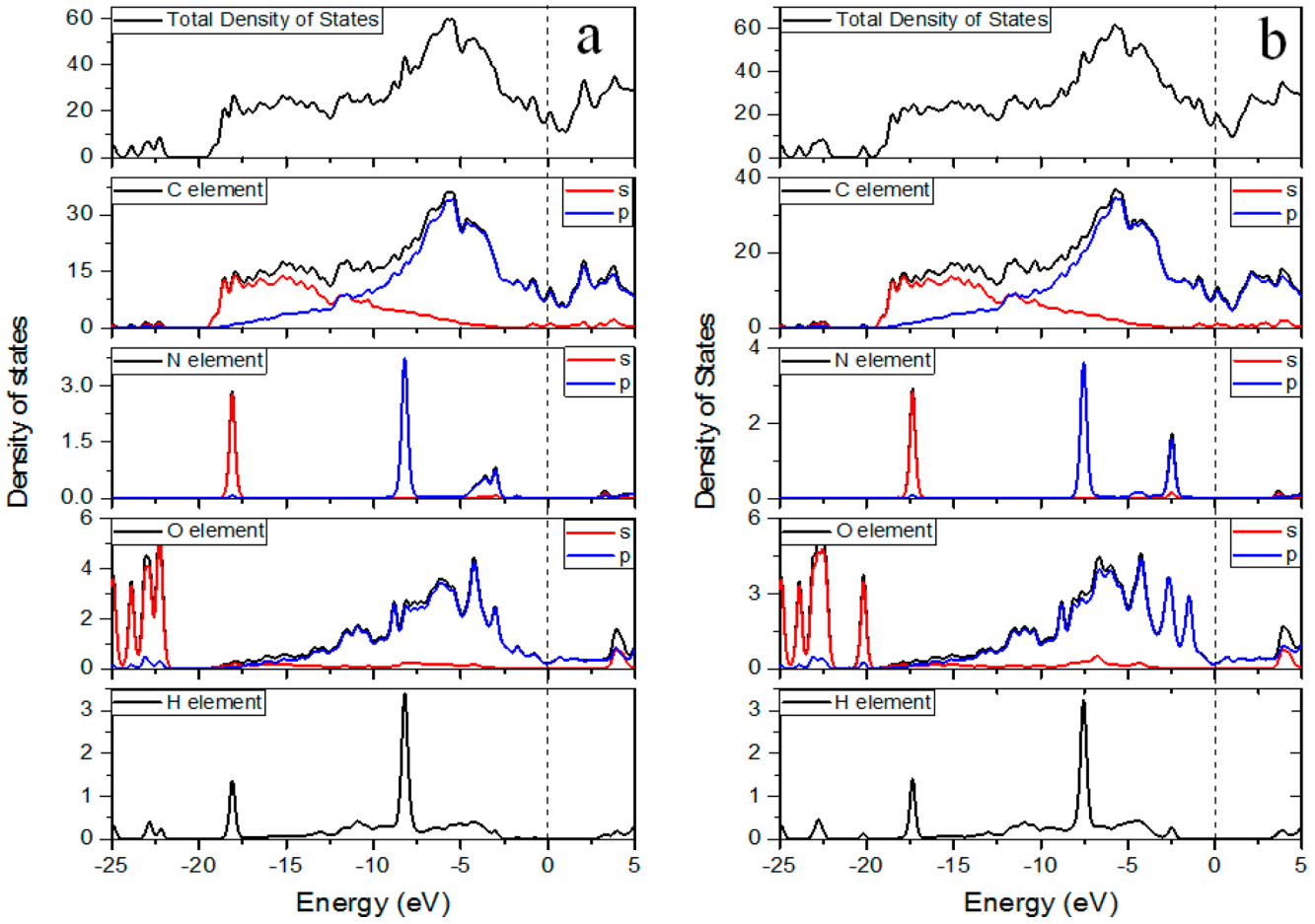

Figure 7. Calculated density of states of mesoporous carbon with (a) −OH at surface, (b) −COOH at surface. The zero of energy is aligned with the top of the valence band. The red and blue lines represent the s and p orbitals of corresponding element.

at surface, respectively) as shown in Figure S15. The broaden upper valence band of NH_3 confirms the chemical bond between hydroxyl base and leads to a higher absorption energy of about 0.5 eV between NH_3 and −OH. On the basis of the calculations, the mesoporous carbon as NH_3 sensors is mainly dependent on the hydroxyl from the carboxyl. As a result, the active sites located on the surface of mesoporous carbon are most likely to be the −COOH groups. According to the theoretical calculations, partial mesopore channels of the mesoporous carbon can be occupied by the bonds between −COOH, −OH groups and NH_3 molecules (4.67 and 3.33 Å respectively, Figure S16d and e), significantly reducing the space of ammonia passage, especially in the cases for small pore size. The hindered diffusion of NH_3 molecules into the mesopores results in inadequate accessible active sites and poor sensing performance for the mesoporous carbon with a smaller pore size, in good agreement with sensing test results. It is worth noting that, the monolithic OMCs (i.e., mesopore size: 9.5 nm) reported previously from Dai group[20] by using Pluronic F127 as a structure-directing agent, a mixture of phloroglucinol and formaldehyde as carbon precursors possess similar surface properties, but our OMCs possess more accessible active sites due to the ordered large pores and highly interconnected pore structure.

The in situ Fourier transform infrared spectroscopy analysis was performed to elucidate the sensing performance of our sample (Figure S17). The mesoporous carbon-PEO_{117}-*b*-PS_{198} materials possess a strong absorption at around 1730 cm^{-1} attributed to −COOH groups.[70] After exposure to 100 ppm of NH_3 for 1 min, the band becomes broad and weakened possibly due to the formation of carboxylate, implying a large amount of active sites located in the carbon framework to yield high sensitive sensing. On the other hand, the unique feature of our OMCs with large mesopores contributes the excellent sensing performance. First, the large and tubular mesopore channels facilitate the rapid diffusion of gas molecules for fast sensing response. Second, the high surface area with numerous acidic active sites enables the adsorption of large amount of gas molecules for ultrahigh sensitivity.

CONCLUSIONS

In summary, a novel solvent evaporation induced micelle fusion−aggregation assembly method has been demonstrated for synthesis of OMCs with 2D hexagonal mesostructure and large cylindrical mesopores by using PEO-*b*-PS copolymers as the templates and RF resin as the carbon source, respectively. The large pore diameter can be readily tunable from 26 to 36 nm, and the specific surface area and pore volume are as high as 571−880 m^2/g and 0.54 cm^3/g, respectively. The obtained large-pore mesoporous carbons can be employed to fabricate nano-devices as NH_3 sensors working at a low temperature and exhibit an excellent sensing performance with a fast response, ultralow limit of detection of 1 ppm, and excellent selectivity. Owing to their good merits of large pores, high surface area and large pore volumes, our OMCs hold a great promising for applications in portable miniaturized devices for ammonia sensing.

DOI: 10.1021/jacs.6b07355
J. Am. Chem. Soc. 2016, 138, 12586−12595

■ ASSOCIATED CONTENT

Supporting Information

The Supporting Information is available free of charge on the ACS Publications website at DOI: 10.1021/jacs.6b07355.

Supporting methods, figures, and tables. (PDF)

■ AUTHOR INFORMATION

Corresponding Authors

*yhdeng@fudan.edu.cn

*dyzhao@fudan.edu.cn

Notes

The authors declare no competing financial interest.

■ ACKNOWLEDGMENTS

This work was supported by the State Key 973 Program of PRC (2013CB934104), the NSF of China (51372041, 51422202, 21673048, 51402049, 51432004, 21210004 and U1463206), the Shanghai Committee of Science and Technology, China (14JC1400700, 14ZR1400600), the "Shu Guang" Project (13SG02), National Youth Top-notch Talent Support Program of China, the Program of Introducing Talents of Discipline to Universities (No. 111-2-04), the Fundamental Research Funds for the Central Universities (No. 2232015D3-06), State Key Laboratory of ASIC & System (2015KF002), and Qatar University grant # QUUG-CAS-DMST-15\16-18. We extend our appreciation to the Deanship of Scientific Research at King Saud University for its funding this Prolific Research group (PRG-1437-32).

■ REFERENCES

(1) Stokstad, E. *Science* **2014**, *343*, 238.

(2) Harrison, P. G.; Willett, M. J. *Nature* **1988**, *332*, 337−339.

(3) Shustova, N. B.; Cozzolino, A. F.; Reineke, S.; Baldo, M.; Dincă, M. *J. Am. Chem. Soc.* **2013**, *135*, 13326−13329.

(4) Zhou, X.; Lee, S. Y.; Xu, Z. C.; Yoon, J. Y. *Chem. Rev.* **2015**, *115*, 7944−8000.

(5) Liu, H. Q.; Kameoka, J.; Czaplewski, D. A.; Craighead, H. G. *Nano Lett.* **2004**, *4*, 671−675.

(6) Feng, L.; Musto, C. J.; Suslick, K. S. *J. Am. Chem. Soc.* **2010**, *132*, 4046−4047.

(7) Modi, A.; Koratkar, N.; Lass, E.; Wei, B. Q.; Ajayan, P. M. *Nature* **2003**, *424*, 171−174.

(8) Li, L.; Yang, Z. B.; Gao, H. J.; Zhang, H.; Ren, J.; Sun, X. M.; Chen, T.; Kia, H. G.; Peng, H. S. *Adv. Mater.* **2011**, *23*, 3730−3735.

(9) Duy, L. T.; Kim, D. J.; Trung, T. Q.; Dang, V. Q.; Kim, B. Y. *Adv. Funct. Mater.* **2015**, *25*, 883−890.

(10) He, Q. Y.; Wu, S. X.; Yin, Z. Y.; Zhang, H. *Chem. Sci.* **2012**, *3*, 1764−1772.

(11) Wang, L. L.; Lou, Z.; Fei, T.; Zhang, T. *J. Mater. Chem.* **2012**, *22*, 4767−4771.

(12) Danesh, E.; Molina-Lopez, F.; Camara, M.; Bontempi, A.; Quintero, A. V.; Teyssieux, D.; Thiery, L.; Briand, D.; de Rooij, N. F.; Persaud, K. C. *Anal. Chem.* **2014**, *86*, 8951−8958.

(13) Ashraf, P. M.; Lalitha, K. V.; Edwin, L. *Sens. Actuators, B* **2015**, *208*, 369−378.

(14) Donato, N.; Latino, M.; Neri, G. In *Carbon Nanotubes—From Research to Applications*; Bianco, S., Ed.; InTech: Rijeka, Croatia, 2011; Ch. 14.

(15) Choi, M. K.; Ryoo, R. *Nat. Mater.* **2003**, *2*, 473−476.

(16) Jiang, H.; Zhang, H. X.; Fu, Y.; Guo, S. J.; Hu, Y. J.; Zhang, L.; Liu, Y.; Liu, H. L.; Li, C. Z. *ACS Nano* **2016**, *10*, 1648−1654.

(17) Fang, Y.; Lv, Y. Y.; Gong, F.; Wu, Z. X.; Li, X. M.; Zhu, H. W.; Zhou, L.; Yao, C.; Zhang, F.; Zheng, G. F.; Zhao, D. Y. *J. Am. Chem. Soc.* **2015**, *137*, 2808−2811.

(18) Wang, X. Q.; Dai, S. *Angew. Chem., Int. Ed.* **2010**, *49*, 6664−6666.

(19) Qiao, Z. A.; Guo, B. K.; Binder, A. J.; Chen, J. H.; Veith, G. M.; Dai, S. *Nano Lett.* **2013**, *13*, 207−212.

(20) Liang, C. D.; Dai, S. *J. Am. Chem. Soc.* **2006**, *128*, 5316−5317.

(21) Tang, J.; Liu, J.; Li, C. L.; Li, Y. Q.; Tade, M. O.; Dai, S.; Yamauchi, Y. *Angew. Chem.* **2015**, *54*, 588−593.

(22) Wu, Z. Y.; Xu, X. X.; Hu, B. C.; Liang, H. W.; Lin, Y.; Chen, L. F.; Yu, S. H. *Angew. Chem., Int. Ed.* **2015**, *54*, 8179−8183.

(23) Niu, W. H.; Li, L. G.; Liu, X. J.; Wang, N.; Liu, J.; Zhou, W. J.; Tang, Z. H.; Chen, S. W. *J. Am. Chem. Soc.* **2015**, *137*, 5555−5562.

(24) Werner, J. G.; Hoheisel, T. N.; Wiesner, U. *ACS Nano* **2014**, *8*, 731−743.

(25) Sakamoto, Y.; Kim, T. W.; Ryoo, R.; Terasaki, O. *Angew. Chem., Int. Ed.* **2004**, *43*, 5231−5234.

(26) Liang, H. W.; Zhuang, X. D.; Brüller, S.; Feng, X. L.; Müllen, K. *Nat. Commun.* **2014**, *5*, 4973.

(27) Wu, R.; Zhang, J. F.; Shi, Y. M.; Liu, D. L.; Zhang, B. *J. Am. Chem. Soc.* **2015**, *137*, 6983−6986.

(28) Sun, Z. K.; Sun, B.; Qiao, M. H.; Wei, J.; Yue, Q.; Wang, C.; Deng, Y. H.; Kaliaguine, S.; Zhao, D. Y. *J. Am. Chem. Soc.* **2012**, *134*, 17653−17660.

(29) Barg, S.; Perez, F. M.; Ni, N.; Pereira, P. d. V.; Maher, R. C.; Garcia-Tuñon, E.; Eslava, S.; Agnoli, S.; Mattevi, C.; Saiz, E. *Nat. Commun.* **2014**, *5*, 4328.

(30) Zhang, J. T.; Zhao, Z. H.; Xia, Z. H.; Dai, L. M. *Nat. Nanotechnol.* **2015**, *10*, 444−452.

(31) Ji, X. L.; Li, K. T.; Nazar, L. F. *Nat. Mater.* **2009**, *8*, 500−506.

(32) Ariga, K.; Vinu, A.; Ji, Q. M.; Ohmori, O.; Hill, J. P.; Acharya, S.; Koike, J.; Shiratori, S. *Angew. Chem., Int. Ed.* **2008**, *47*, 7254−7257.

(33) Lu, C. C.; Liao, K. H. *Sens. Actuators, B* **2010**, *143*, 500−507.

(34) Liu, J.; Yang, T. Y.; Wang, D. W.; Lu, G. Q.; Zhao, D. Y.; Qiao, S. Z. *Nat. Commun.* **2013**, *4*, 2798.

(35) Orilall, M. C.; Matsumoto, F.; Zhou, Q.; Sai, H.; Abruna, H. D.; DiSalvo, F. J.; Weisner, U. *J. Am. Chem. Soc.* **2009**, *131*, 9389−9395.

(36) Schuster, J.; He, G.; Mandlmeier, B.; Yim, T.; Lee, K. T.; Bein, T.; Nazar, L. F. *Angew. Chem., Int. Ed.* **2012**, *51*, 3591−3595.

(37) Fulvio, P. F.; Mayes, R. T.; Wang, X. Q.; Mahurin, S. M.; Bauer, J. C.; Presser, V.; Mcdonough, J.; Gogotsi, Y.; Dai, S. *Adv. Funct. Mater.* **2011**, *21*, 2208−2215.

(38) Zhi, J.; Zhao, W.; Liu, X. Y.; Chen, A. R.; Liu, Z. Q.; Huang, F. Q. *Adv. Funct. Mater.* **2014**, *24*, 2013−2019.

(39) Liu, R. L.; Shi, Y. F.; Wan, Y.; Meng, Y.; Zhang, F. Q.; Gu, D.; Chen, Z. X.; Tu, B.; Zhao, D. Y. *J. Am. Chem. Soc.* **2006**, *128*, 11652−11662.

(40) Deng, Y. H.; Yu, Y.; Wan, Y.; Shi, Y. F.; Meng, Y.; Gu, D.; Zhang, L. J.; Huang, Y.; Liu, C.; Wu, X. J.; Zhao, D. Y. *J. Am. Chem. Soc.* **2007**, *129*, 1690−1697.

(41) Lim, E.; Kim, H.; Jo, C.; Chun, J.; Ku, K.; Kim, S.; Lee, H. I.; Nam, I. S.; Yoon, S.; Kang, K. *ACS Nano* **2014**, *8*, 8968−8978.

(42) Liang, C. D.; Hong, K. L.; Guiochon, G. A.; Mays, J. W.; Dai, S. *Angew. Chem., Int. Ed.* **2004**, *43*, 5785−5789.

(43) Rodriguez, A. T.; Li, X. F.; Wang, J.; Steen, W. A.; Fan, H. Y. *Adv. Funct. Mater.* **2007**, *17*, 2710−2716.

(44) Wei, J.; Wang, H.; Deng, Y. H.; Sun, Z. K.; Shi, L.; Tu, B.; Luqman, M.; Zhao, D. Y. *J. Am. Chem. Soc.* **2011**, *133*, 20369−20377.

(45) Wang, C.; Wei, J.; Yue, Q.; Luo, W.; Li, Y. H.; Wang, M. H.; Deng, Y. H.; Zhao, D. Y. *Angew. Chem., Int. Ed.* **2013**, *52*, 11603−11606.

(46) Hwang, J. K.; Woo, S. H.; Shim, J. M.; Jo, C. S.; Lee, K. T.; Lee, J. W. *ACS Nano* **2013**, *7*, 1036−1044.

(47) Luo, W.; Li, Y. H.; Dong, J. P.; Wei, J.; Xu, J. Q.; Deng, Y. H.; Zhao, D. Y. *Angew. Chem., Int. Ed.* **2013**, *52*, 10505−10510.

(48) Lee, J. W.; Christopher, O. M.; Warren, S. C.; Kamperman, M.; Disalvo, F. J.; Wiesner, U. *Nat. Mater.* **2008**, *7*, 222−228.

(49) Dunphy, D. R.; Sheth, P. H.; Garcia, F. L.; Brinker, C. J. *Chem. Mater.* **2015**, *27*, 75−84.

(50) Richman, E. K.; Kang, C. B.; Brezesinski, T.; Tolbert, S. H. *Nano Lett.* **2008**, *8*, 3075−3079.

(51) Li, Y. H.; Luo, W.; Qin, N.; Dong, J. P.; Wei, J.; Li, W.; Feng, S. S.; Chen, J. C.; Xu, J. Q.; Elzatahry, A. A.; Es-Saheb, M. H.; Deng, Y. H.; Zhao, D. Y. *Angew. Chem., Int. Ed.* **2014**, *53*, 9035−9040.
(52) Takai, A.; Yamauchi, Y.; Kuroda, K. *J. Am. Chem. Soc.* **2010**, *132*, 208−214.
(53) Liu, C.; Deng, Y. H.; Liu, J.; Wu, H. H.; Zhao, D. Y. *Microporous Mesoporous Mater.* **2008**, *116*, 633−640.
(54) Yue, Z. R.; Jiang, W.; Wang, L. J.; Gardner, S. D.; Pittman, C. U., Jr *Carbon* **1999**, *37*, 1785−1796.
(55) Gardner, S. D.; Singamsetty, C. S. K.; Booth, G. L.; He, G. R.; Pittman, C. U., Jr *Carbon* **1995**, *33*, 587−595.
(56) Kong, J.; Franklin, N. R.; Zhou, C. W.; Chapline, M. G.; Peng, S.; Cho, K. J.; Dai, H. J. *Science* **2000**, *287*, 622−625.
(57) Collins, P. G.; Bradley, K.; Ishigami, M.; Zettl, A. *Science* **2000**, *287*, 1801−1804.
(58) Snow, E. S.; Perkins, F. K. *Nano Lett.* **2005**, *5*, 2414−2417.
(59) Christie, S.; Scorsone, E.; Persaud, K.; Kvasnik, F. *Sens. Actuators, B* **2003**, *90*, 163−169.
(60) Yan, Li.; Hodak, M.; Lu, W. C.; Bernholc, J. *Carbon* **2016**, *101*, 177−183.
(61) Guerin, H.; Le Poche, H.; Pohle, R.; Bernard, L. S.; Buitrago, E.; Ramos, R.; Dijon, J.; Ionescu, A. M. *Carbon* **2014**, *78*, 326−338.
(62) Arab, M.; Berger, F.; Picaud, F.; Ramseyer, C.; Glory, J.; Mayne-L'Hermite, M. *Chem. Phys. Lett.* **2006**, *433*, 175−181.
(63) Quang, N. H.; Trinh, M. V.; Lee, B. H.; Huh, J. S. *Sens. Actuators, B* **2006**, *113*, 341−346.
(64) Hoa, N. D.; Quy, N. V.; Cho, Y.; Kim, D. *Sens. Actuators, B* **2007**, *127*, 447−454.
(65) Hoa, N. D.; Quy, N. V.; Cho, Y.; Kim, D. *Sens. Actuators, B* **2009**, *135*, 656−663.
(66) Wang, L. C.; Tang, K. T.; Teng, I. J.; Kuo, C. T.; Ho, C. L.; Kuo, H. W.; Su, T. H.; Yang, S. R.; Shi, G. N.; Chang, C. P. *Sensors* **2011**, *11*, 7763−7772.
(67) Yavari, F.; Chen, Z. P.; Thomas, A. V.; Ren, W. C.; Cheng, H. M.; Koratkar, N. *Sci. Rep.* **2011**, *1*, 166.
(68) Wang, D. H.; Hu, Y.; Zhao, J. J.; Zeng, L. L.; Tao, X. M.; Chen, W. *J. Mater. Chem. A* **2014**, *2*, 17415−17420.
(69) Paul, R. K.; Badhulika, S.; Saucedo, N. M.; Mulchandani, A. *Anal. Chem.* **2012**, *84*, 8171−8178.
(70) Wu, Z. X.; Webley, P. A.; Zhao, D. Y. *Langmuir* **2010**, *26*, 10277−10286.

DOI: 10.1021/jacs.6b07355
J. Am. Chem. Soc. 2016, 138, 12586−12595